Additional Investigations of a New Kinetic Method To Follow Transition-Metal Nanocluster Formation, Including the Discovery of Heterolytic Hydrogen Activation in Nanocluster Nucleation Reactions

Jason A. Widegren, John D. Aiken, III, Saim Özkar, and Richard G. Finke*

Department of Chemistry, Colorado State University, Ft. Collins, Colorado 80523

Received August 24, 2000. Revised Manuscript Received November 2, 2000

A few years ago we developed a new kinetic method for following transition-metal nanocluster formation in which the resultant nanocluster's catalytic activity was used as a reporter reaction via the pseudoelementary step concept. This method in turn yielded insights into a new, broadly applicable mechanism of nanocluster formation under H_2 consisting of (a) slow, continuous nucleation, **A** → **B**, followed by (b) fast autocatalytic surface growth, **A** + **B** → 2**B** (**A** = the nanocluster precursor, $[Bu_4N]_5Na_3[(1,5\text{-COD})Ir{\cdot}P_2W_{15}Nb_3O_{62}]$, **B** = the resultant nanocluster's surface metal atoms), in which the nanocluster behaves as a "living metal polymer". Herein, this new kinetic method is investigated and tested further: (i) by following the $Ir(0)_{\sim 300}$ nanocluster's kinetics of formation more directly via the H_2 uptake reaction of the $[Bu_4N]_5Na_3[(1,5\text{-COD})Ir{\cdot}P_2W_{15}Nb_3O_{62}]$ precursor—does this also show an autocatalytic H_2 uptake curve?; (ii) by seeing if the predicted initially small, then larger (past the induction period) sizes of the nanoclusters are verifiable directly by TEM; (iii) by testing commercial nonlinear least-squares software (Microcal's ORIGIN) in the kinetic analysis and with the goal of making the new kinetic method readily available to others; (iv) by showing when it is necessary to correct for the solvent vapor pressure, and how to do so, in the H_2 pressure-loss measurements when more volatile solvents such as acetone are used in the nanocluster formation reaction; (v) by showing whether the new kinetic method can be successfully used in other nanocluster formation reactions of different metals and for more difficult reactions such as arene hydrogenation; and (v) by numerical integration simulations of the first 45 or so steps in the nanocluster formation reaction—does this atomically detailed mechanism show autocatalysis or not, and if so can it be fit by the **A** → **B**, **A** + **B** → 2**B** mechanism? Tests of each of the issues (i)−(v) are reported in the present contribution. Finally, (vi) the new kinetic method has been exploited to yield insights into higher valent metals that undergo nucleation under H_2, namely, to discover and report for the first time the significance of heterolytic hydrogenation activation, with its requirement for added base in the nanocluster formation reactions of higher valent, electrophilic metals such as Pd(II), Pt(IV), Ru(III), Rh(III), Ag(I), Au(III), Cu(II), and Ir(III).

Introduction

Nanoparticles[1] are an important, very active area of modern materials science. Of special interest is the synthesis of near-monodisperse (i.e., ≤±15%)[2] nanoclusters where their size, size distribution, composition, and shape are controlled via designed, rational syntheses. Hindering accomplishment of this important objective, however, is the relative dearth of kinetic and mechanistic information on the formation pathway(s) of modern, compositionally well-defined transition-metal nanoclusters.[3,4] Our recent nanocluster reviews[2] reveal three main reasons for this dearth of kinetic and

* To whom correspondence should be addressed. E-mail: Rfinke@lamar.colostate.edu.

(1) Reviews on nanoclusters; see also our own reviews elsewhere[2]: (a) Jena, P.; Rao B. K.; Khanna, S. N. *Physics and Chemistry of Small Clusters*; Plenum: New York, 1987. (b) Andres, R. P.; Averback, R. S.; Brown, W. L.; Brus, L. E.; Goddard, W. A., III; Kaldor, A.; Louie, S. G.; Moscovits, M.; Peercy, P. S.; Riley, S. J.; Siegel, R. W.; Spaepen, F.; Wang, Y. *J. Mater. Res.* **1989**, *4*, 704. This is a Panel Report from the United States Department of Energy, Council on Materials Science on "Research Opportunities on Clusters and Cluster-Assembled Materials". (c) Thomas, J. M. *Pure Appl. Chem.* **1988**, *60*, 1517. (d) Henglein, A. *Chem. Rev.* **1989**, *89*, 1861. (e) A superb series of papers, complete with a record of the insightful comments by the experts attending the conference, is available in: *Faraday Discuss.* **1991**, *92*, 1−300. (f) Bradley, J. S. In *Clusters and Colloids. From Theory to Applications*; Schmid, G., Ed.; VCH: New York, 1994; pp 459−544. (g) Schmid, G. In *Aspects of Homogeneous Catalysis*; Ugo, R., Ed.; Kluwer: Dordrecht, 1990; Chapter 1. (h) Bönnemann, H.; Braun, G.; Brijoux, W.; Brinkmann, R.; Tilling, A. S.; Seevogel, K.; Siepen, K. *J. Organomet. Chem.* **1996**, *520*, 143−162, and the collection of "key publications" cited as refs 2−61 therein. (i) Raithby, P. R. *Platinum Met. Rev.* **1998**, *42*, 146. (j) Schmid, G.; Bäumle, M.; Geerkens, M.; Heim, I.; Osemann, C.; Sawitowski, T. *Chem. Soc. Rev.* **1999**, *28*, 179.

(2) (a) See elsewhere for a review of nanocluster catalysis that includes necessary key terms and definitions of the following:[2b] nanoclusters; traditional colloids; monodisperse and near-monodisperse nanoparticles; "magic number" (i.e., full shell and thus enhanced stability) nanoclusters; Schwartz's updated definition of homogeneous vs heterogeneous catalysts; inorganic ("charge") and organic ("steric") stabilization mechanisms for colloids and nanoparticles; plus a review of the Bu_4N^+ and polyoxoanion-stabilized $Ir(0)_{\sim 300}$ nanoclusters discussed herein. A review focusing on nanocluster catalysis is also available,[2c] as is a recent review emphasizing the important components of nano-*molecular* chemistry and its advantages over nanocolloidal or nanomaterials chemistry:[2d] (b) Aiken, J. D., III; Lin, Y.; Finke, R. G. *J. Mol. Catal. A: Chem.* **1996**, *114*, 29−51. (c) Aiken, J. D., III.; Finke, R. G. *J. Mol. Catal. A: Chem.* **1999**, *145*, 1. (d) Finke, R. G. In *Metal Nanoparticles: Synthesis, Characterization and Applications*; Feldheim, D. L., Foss, C. A., Jr., Eds.; Marcel Dekker: New York, 2001, in press ("Transition-Metal Nanoclusters: Solution-Phase Synthesis, then Characterization and Mechanism of Formation, of Polyoxoanion- and Tetrabutylammonium-Stabilized Nanoclusters").

10.1021/cm0006852 CCC: $20.00
Published on Web 01/03/2001

mechanistic studies: (i) only recently have the first examples of modern, *compositionally fully defined*, prototype transition-metal nanoclusters appeared, that is, ones suitable for in-depth kinetic and mechanistic studies.[1,2b,5] An example is the $P_2W_{15}Nb_3O_{62}^{9-}$ polyoxoanion- and Bu_4N^+-stabilized, 20 ± 3 Å $Ir(0)_{\sim 190-450}$ (hereafter $Ir(0)_{\sim 300}$)[2,5] nanoclusters that we first reported in 1994 (Figure 1), nanoclusters which are synthesized from the well-established precatalyst[6] $[Bu_4N]_5Na_3[(1,5\text{-COD})Ir{\cdot}P_2W_{15}Nb_3O_{62}]$ by reduction under H_2. Second, (ii) the available ways to monitor the formation of nanoclusters in real time are limited;[7] and hence (iii) only more recently have mechanistic chemists begun to tackle this area.[4]

In 1997 we reported[8] the development of an indirect—but continuous, easy, highly quantitative, and thus powerful—method to monitor the formation, eq 1, of the

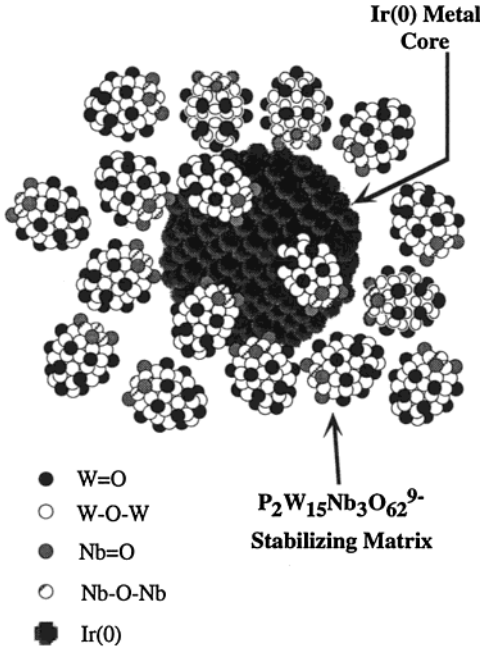

Figure 1. Idealized, roughly to scale representation of a $P_2W_{15}Nb_3O_{62}^{9-}$ polyoxoanion and Bu_4N^+-stabilized $Ir(0)_{\sim 300}$ nanocluster, $[Ir(0)_{\sim 300}(P_4W_{30}Nb_6O_{123}^{16-})_{\sim 33}]$ $(Bu_4N)_{\sim 300}Na_{\sim 228}$. The Ir(0) atoms are known (by electron diffraction) to be cubic close packed as shown.[5] For the sake of clarity, only 17 polyoxoanions are shown, the polyoxoanion is shown in its monomeric, $P_2W_{15}Nb_3O_{62}^{9-}$ form (and not as its Nb−O−Nb bridged, anhydride, $P_4W_{30}Nb_6O_{123}^{16-}$ form that is known to be present[5]), and the ≈300 Bu_4N^+ and ≈228 Na^+ cations have been deliberately omitted. The highly catalytically active, bottleable, redissolvable $Ir(0)_{\sim 300}$ nanoclusters[2,5,8] have been extensively characterized by TEM, electron diffraction, electrophoresis, elemental analysis, ultracentrifugation MW determination, and IR and UV−visible spectroscopy.[2,5] The polyoxoanion component of our nanoclusters is without precedent in any previous type of nanocluster or colloid, a point that is fortified by the knowledge that the required type of basic polyoxoanion (i.e., with surface oxygen basicity) is new.[2]

(3) Classic papers on nanocluster formation: (a) LaMer's mechanism of sulfur sol formation, consisting of homogeneous nucleation from supersaturated solution followed by diffusive, agglomerative growth (a mechanism quite different than that discovered for transition-metal nanocluster formation via the kinetic methods reported herein and as summarized elsewhere[8]): LaMer, V. K.; Dinegar, R. H. *J. Am. Chem. Soc.* **1950**, *72*, 4847; LaMer, V. K. *Ind. Eng. Chem.* **1952**, *44*, 1270. (b) Turkevich's mechanistic studies: Turkevich, J.; Stevenson, P. C.; Hillier, J. *Faraday Discuss. Chem. Soc.* **1951**, *11*, 55. (c) Reiss, H. *J. Chem. Phys.* **1951**, *19*, 482. (d) A comprehensive list of the 19 prior papers since 1950 plus the 6 pulse radiolysis papers cited below,[3f−i] which provide mechanistic data on colloid or nanocluster formation, has been compiled in Table A of the Supporting Information elsewhere[8] for the interested reader, along with brief summaries covering the contents of each paper. (e) Listed in refs 3f−i below are studies of pulse radiolysis reduction of Ag^+ to $Ag(0)_n$ nanoclusters. These studies[3f−i] (which are somewhat buried in the pulse radiolysis and Ag photographic process literature) were not noted previously,[8] only because they were not uncovered via our earlier literature search of nanocluster formation kinetic and mechanistic studies.[8] These Ag^+ reduction studies are, however, relevant to the present and our earlier kinetic and mechanistic work,[8] even though (i) Ag^+ and Ag(0) are not, strictly speaking, transition metals (do not have *partially filled* d or f shells), (ii) the pulsed reduction nature of the pulse radiolysis method bears little resemblance to a continuous reduction method such as the use of H_2 herein; and (iii) the pulse radiolysis method suffers from not producing useful quantities of isolable nanoclusters (and thus uncharacterized are the nanocluster product's composition, size dispersion, and so on). In addition, and although autocatalysis is occasionally mentioned therein,[3f−i] (iv) there is no unequivocal, compelling kinetic evidence for autocatalysis (nor identification or semiquantitative treatment of issues such as the fraction of surface atoms). Nevertheless, the following proposed steps in the Ag(0) and our Ir(0) systems are formally analogous mechanistically as surface-growth processes: $Ag(0)_n + Ag^+ + SPV^{-\bullet} \rightarrow Ag(0)_{n+1} + SPV$ (where SPV = sulfonato propyl viologen); $Ir(0)_n + [(1,5\text{-COD})Ir^{I}{\cdot}P_2W_{15}Nb_3O_{62}]^{8-} + 2.5H_2 \rightarrow Ir(0)_{n+1}$ + cyclooctane + H^+ + $[P_2W_{15}Nb_3O_{62}]^{9-}$. Note that the reduction of Ag^+ is proposed to occur only after formation of $Ag(0)_n{\cdot}Ag^+$ (i.e., after coordination of Ag^+ to the $Ag(0)_n$ surface), which differs from the $Ir(0)_n$ case only in that activation of xH_2 on the $Ir(0)_n$ surface to give $Ir(0)_n{\cdot}(H)_{2x}$ probably occurs first, that is, prior to the reaction of the resultant $Ir(0)_n{\cdot}(H)_{2x}$ with $[(1,5\text{-COD})Ir^{I}(\text{solvent})]^+$ and/or $[(1,5\text{-COD})Ir^{I}{\cdot}P_2W_{15}Nb_3O_{62}]^{8-}$. (f) Mostafavi, M.; Marignier, J. L.; Amblard, J.; Belloni, J. *Radiat. Phys. Chem.* **1989**, *34*, 605. Mostafavi, M.; Marignier, J. L.; Amblard, J.; Belloni, J. *Z. Phys. D* **1989**, *12*, 31. Belloni, J.; Amblard, J.; Marignier, J. L.; Mostafavi, M. In *Clusters of Atoms and Molecules, II: Solvation and Chemistry of Free Clusters, and Embedded, Supported and Compressed Clusters*; Haberland, H., Ed.; Springer-Verlag: Berlin, 1994; Vol. 2, p 290. (g) Henglein, A.; Tausch-Treml, R. *J. Colloid Interface Sci.* **1981**, *80*, 84. (h) Ershov, B. G.; Kartashev, N. I. *Russ. Chem. Bull.* **1995**, *44*, 29. (i) Rabani, J.; Fessenden, R. W.; Sassoon, R. E. *J. Phys. Chem.* **1988**, *92*, 2379.

(4) More recent mechanistic investigations of transition-metal nanocluster formation are the following: (a) our 1997 study;[8] (b) Petroski, J. M.; Wang, Z. L.; Green, T. C.; El-Sayed, M. A. *J. Phys. Chem. B* **1998**, *102*, 3316. (c) Henglein, A.; Giersig, M. *J. Phys. Chem. B* **2000**, *104*, 6767. Note that this paper misquotes our 1997 paper[8] when it says: "It seems probable that reduction by H_2 does not proceed through intermediate *free atom*s (i.e., via naked Ir(0)), as has been postulated.[8] (The parenthetical comment, and the italics, have been added. Reference 8 is to our 1997 mechanistic paper, which just happens to also be ref 8 herein.[8]) In fact, we specifically worried about the high, unstable energetics of Ir(0) formation in footnotes 10, 43a, 44, and 45 of our paper. We concluded that *highly ligated, and thus stabilized, Ir(0)L_y,*—not naked Ir(0) atoms as (mis)quoted above[4c]—is what our evidence suggests. Also made elsewhere in footnote 43d is the point that in general and energetically speaking, one wants Ir−Ir bond formation to proceed reduction to $Ir(0)_x{\cdot}L_y$ whenever possible.[8] Note that our published data are compelling in requiring the formation of $Ir(0)L_y$ or $Ir(0)_x{\cdot}L_y$ species *somewhere along the reaction coordinate.* Nevertheless, Henglein's intuition that there may need to be intermediates other than $Ir(0)L_x$ prior to $Ir(0)_x{\cdot}L_y$ along the reaction pathway may well be right. The one intriguing possibility that we have been able to come up with for such an intermediate is under investigation. (d) See also the related topic of the mechanisms of formation of semiconductor nanocrystals: Peng, X.; Wickham, J.; Alivisatos, A. P. *J. Am. Chem. Soc.* **1998**, *120*, 5343. Chen, C.-C.; Herhold, A. B.; Johnson, C. S.; Alivisatos, A. P. *Science* **1997**, *276*, 398.

(5) (a) Lin, Y.; Finke, R. G. *J. Am. Chem. Soc.* **1994**, *116*, 8335. (b) Lin, Y.; Finke, R. G. *Inorg. Chem.* **1994**, *33*, 4891. (c) The *average* composition of the $Ir(0)_{\sim 300}$ and $Ir(0)_{\sim 900}$ nanoclusters were demonstrated to be $[Ir(0)_{\sim 300}(P_4W_{30}Nb_6O_{123}^{16-})_{\sim 33}](Bu_4N)_{\sim 300}Na_{\sim 228}$ and $[Ir(0)_{\sim 900}(P_4W_{30}Nb_6O_{123}^{16-})_{\sim 60}](Bu_4N)_{\sim 660}Na_{\sim 300}$, respectively. Note that the $P_2W_{15}Nb_3O_{62}^{9-}$ has formed its anhydride, in the presence of the 1 equiv of H^+ produced in the nanocluster formation reaction, via the following reaction: $2P_2W_{15}Nb_3O_{62}^{9-} + 2H^+ \rightarrow H_2O + [(P_2W_{15}Nb_3O_{61})_2{-}O]^{16-}$ (see elsewhere for additional discussion of this point).[5a,b] (d) Additional characterization studies of the $Ir(0)_{\sim 300}$ nanoclusters by HR-TEM, HR-TEM of nanoclusters deposited on SiO_2 spheres, STM, and if possible, mass spectroscopy are nearing completion and will be reported in due course, Aiken, J. D., III; Finke, R. G., unpublished results. (e) The present paper is Part VII in a series of papers focusing on the kinetics and mechanism of nanocluster formation reactions.[5,8,12,13,20,22]

(6) (a) Pohl, M.; Lyon, D. K.; Mizuno, N.; Nomiya, K.; Finke R. G. *Inorg. Chem.* **1995**, *34*, 1413. (b) Weiner, H.; Aiken, J. D., III; Finke, R. G. *Inorg. Chem.* **1996**, *35*, 7905.

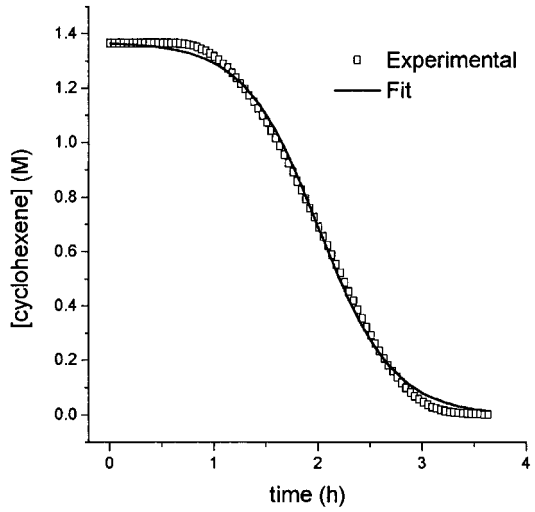

Figure 2. Typical cyclohexene loss vs time curve and curve fit demonstrating the generally excellent fit to the nucleation plus autocatalysis, then hydrogenation, three-step kinetic model in eqs 2a−2c. The first ≈30 min of the pressure data was back-extrapolated to remove the rise seen due to the acetone solvent's vapor pressure re-equilibration; see the section that follows on this topic for further details. The observed data points do not show error bars from the high-precision pressure transducer measurement of the H_2 consumption because they are ±0.01 psig (which translates to ± 0.001 M cyclohexene) and thus are too small to depict (i.e., are smaller than the width of the line shown). The error bars on the rate constants k_1 and k_2 that result from the kinetic analysis and curve fits, vide infra, are typically 10−15%. The deviation of the curve fit from the data late in the reaction is also understood, being due to cyclohexene concentration nearing zero and the resultant failure of step 2c to be faster than steps 2a and 2b, vide infra (i.e., the expected failure at low [cyclohexene] of the pseudoelementary concept used to follow the nanocluster formation reaction, vide infra). Note that these kinetic curves and their underlying nucleation and autocatalytic growth are sensitive functions of the exact water content and purity/source of the acetone solvent,[5b] the H_2 pressure, the temperature, the presence of additional $[P_2W_{15}Nb_3O_{62}]^{9-}$ polyoxoanion, trace O_2, and other variables,[8] factors that must be considered when comparing individual kinetic curves and their k_1 and k_2 rate constants (vide infra).

Ir(0) transition-metal nanoclusters in Figure 1 via their catalytic hydrogenation (H_2 uptake) activity (Figure 2). The new method exploited the concept of *pseudoelementary*[9] reaction steps, eqs 2a−2d (where **A** in eqs 2a−2d is the precatalyst, $[Bu_4N]_5Na_3[(1,5\text{-COD})Ir{\cdot}P_2W_{15}Nb_3O_{62}]$,

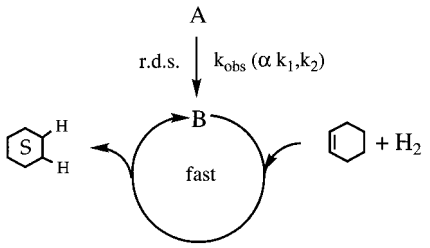

Figure 3. Simplified illustration of how transition-metal nanocluster formation is monitored via the fast, follow-up catalytic reaction of cyclohexene hydrogenation. As before, **A** is the precatalyst, $[Bu_4N]_5Na_3[(1,5\text{-COD})Ir{\cdot}P_2W_{15}Nb_3O_{62}]$, and **B** is the growing $Ir(0)_n$ nanocluster catalyst.

and **B** is the catalyst composed of the Ir(0) surface sites on the near-monodisperse[2] distribution of developing nanoclusters, vide infra).

$$300[(1,5\text{-COD})Ir{\cdot}P_2W_{15}Nb_3O_{62}]^{8-} + 750H_2 \rightarrow Ir(0)_{\sim 300}{\cdot}(P_2W_{15}Nb_3O_{62}{}^{9-})_{\sim 66} + 300\text{cyclooctane} + 300H^+ + \sim 234[P_2W_{15}Nb_3O_{62}]^{9-} \quad (1)$$

$$x[\mathbf{A} \xrightarrow[H_2]{k_1} \mathbf{B}] \quad (2a)$$

$$(1-x)[\mathbf{A} + \mathbf{B} \xrightarrow[H_2]{k_2} 2\mathbf{B}] \quad (2b)$$

$$\sim 1400[\mathbf{B} + \text{cyclohex}\textit{ene} + H_2 \xrightarrow{k_3} \mathbf{B} + \text{cyclohex}\textit{ane}] \quad (2c)$$

$$\text{SUM: } \mathbf{A} + \sim 1400\text{cyclohex}\textit{ene} + \sim 1400H_2 \xrightarrow{k_{obs}} \mathbf{B} + \sim 1400\text{cyclohex}\textit{ane} \quad (2d)$$

In consideration of eq 2d, the reaction obtained by summing the three steps outlined in eqs 2a−2c reveals that eq 2d is an illustrative example of the concept that Noyes has termed a pseudoelementary step.[9] If the third step, eq 2c, is fast on the time scale of the first and second steps, then the kinetics of the overall reaction, eq 2d, will be those of steps 1 and 2 only—*the desired nanocluster formation reactions*. This is shown in a perhaps more intuitive way in Figure 3. In other words, step 2d can then be treated and used kinetically as equivalent to an elementary step, even though step 2d is obviously not elementary—but is pseudoelementary—because it is composed of the three steps shown, eqs 2a−2c.

Experimentally, the excellent fit to the data using eqs 2a−2c requires that the third step, eq 2c, be fast in comparison to the first two steps, eqs 2a and 2b. In addition, we have confirmed experimentally the prediction that rate constants k_1 and k_2 for the nucleation and autocatalytic surface growth pseudoelementary steps are *zero order* with respect to cyclohexene concentration under the reaction conditions—that is, eq 2c involving cyclohexene has been shown to be fast as required to follow the growth of the nanoclusters via the pseudoelementary step, eq 2d.[8,10]

Note also that *only* if an autocatalytic step, $\mathbf{A} + \mathbf{B} \rightarrow 2\mathbf{B}$, specifically eq 2b, is included have we been able to come even close to fitting the observed kinetic data

(7) (a) The detection of nanocluster sizes and size distributions is most commonly done by TEM (transmission electron microscopy), although reports of changes induced by the TEM beam are fairly frequent;[1] additional lead references of TEM-induced changes of nanoclusters are provided in ref 18 elsewhere.[5a] One might believe that light scattering is the method of choice for size-distribution monitoring, but this is really only 100% true *if* a single-size, monodispersed nanocluster is present.[7b] (b) Briefly, the reason that light scattering is not the method of choice when a distribution of nanocluster sizes is present is that it involves a fit to a multiexponential function (i.e., instead of a single exponential or function) and then a nonlinear least-squares fit. Hence, the resulting solution cannot be guaranteed to be the true global minimum for the problem. We thank Dr. Jess Wilcoxon of Sandia National Laboratories for his expert discussions on this point.

(8) Watzky, M. A.; Finke, R. G. *J. Am. Chem. Soc.* **1997**, *119*, 10382.

(9) A *pseudoelementary step* is a term invented by Professor Richard Noyes, at the University of Oregon, for dealing with complex (oscillating) reactions. For an introduction to the concept of pseudoelementary reactions, a concept created for and often necessary with the kinetics of more complex systems, see the pioneering work of Professor Noyes and co-workers: (a) Noyes, R. M.; Field, R. J. *Acc. Chem. Res.* **1977**, *10*, 214. (b) Noyes, R. M.; Field, R. J. *Acc. Chem. Res.* **1977**, *10*, 273. (c) Field, R. J.; Noyes, R. M. *Nature* **1972**, *237*, 390.

(Figure 2), as explained in greater detail elsewhere.[8,11] This result is intuitive as well in that we know of no other kinetic function that will allow a reaction to sit seemingly "dormant" for an hour, but then "turn on" and go to completion in a mere additional 2 h (Figure 2). Confirming the apparent uniqueness of autocatalysis in explaining the kinetic data in Figure 2, we have also demonstrated (using numerical integration methods) that we were unable to find empirically any function other than autocatalysis that even comes close to fitting the observed kinetic curves.[11]

Our 1997 kinetic and mechanistic investigation of transition-metal nanocluster formation under H_2 also confirmed, by a second more direct (albeit less convenient and less precise) GLC method, that the use of the pseudoelementary step method indeed works and does so quantitatively, giving the exact same rate constants k_1 and k_2 within experimental error as the pseudoelementary step method. The details of the GLC data analysis include verification of the mathematically required stoichiometry factor (the 1400 in eq 2c) and how to handle the changing fraction of surface atoms on the nanocluster (the "scaling factor", $(1 + x_{\text{growth}})/2$, shown in part B of Scheme 1, that is, the mathematics needed to correct for the fact that the true growth reaction is not exactly $\mathbf{A} + \mathbf{B} \rightarrow 2\mathbf{B}$ but, instead, involves $n \rightarrow n + 1$ for $\mathbf{A} + \text{Ir}(0)_n \rightarrow \text{Ir}(0)_{n+1}$).[8] These important details are available both in the Supporting Information to the present paper as well as in our 1997 paper[8] for the convenience of the interested reader.

The end result of our kinetic and mechanistic studies is a more quantitative, more exact mechanistic description of nanocluster formation as summarized schematically in the minimal, Occam's Razor mechanism shown in Scheme 1. Independent evidence for a diffusive, agglomerative growth step in competition with the autocatalytic surface growth (i.e., and as a function of H_2 pressure as the mechanism in Scheme 1 predicts) has also been published.[12] The availability for the first time of a convenient, facile method for following nanocluster formation allowed us to determine the effects on nanocluster nucleation (k_1) and growth (k_2) of reagents such as H_2O, H^+, added polyoxoanion, and changes in temperature.[8] Application of the new kinetic method also yielded a mechanistic basis for how and why "magic number" nanoclusters tend to form (as a natural consequence of autocatalytic surface growth[13]),

Scheme 1. Pictorial View of the Proposed, Minimum Mechanism of Formation of the Ir(0) and Other Transition-Metal Nanoclusters Prepared under H_2[8]

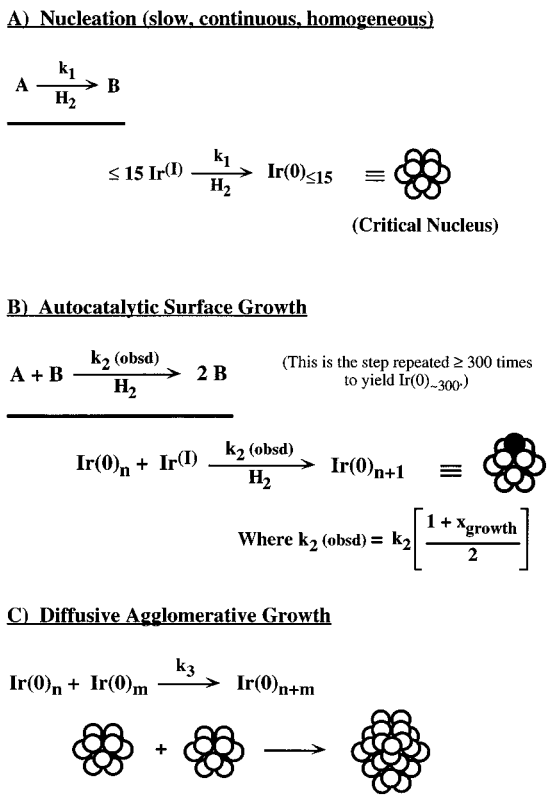

insights into the concept of "living metal polymer" growth of nanoclusters and all its implications for size- and shape control,[13] and the first rational prescription for the synthesis of all possible geometric isomers of onion-shell, bi-, tri-, and higher multimetallic nanoclusters.[13]

Despite the considerable success of the kinetic and mechanistic studies summarized above, several important questions remained unanswered, questions that require experimental scrutiny. Can one follow the nanocluster formation reaction directly in the absence of cyclohexene substrate, and by a method that yields precise kinetic data? If so, does that method also produce a sigmoidal kinetic curve? Can a curve directly monitoring the conversion of $[Bu_4N]_5Na_3[(1,5\text{-COD})Ir{\cdot}P_2W_{15}Nb_3O_{62}]$ under H_2 into nanoclusters be fit by the nucleation and autocatalytic growth mechanism with its k_1 and k_2 rate constants? Can the nanocluster sizes implied by the mechanism in Scheme 1 be verified directly by transmission electron microscopy (TEM) studies, namely, smaller nanoclusters initially then larger nanoclusters as time passes and as the autocatalytic surface growth mechanism operates? Is there commercial software that can be used to do the nonlinear least-squares curve fitting of the data in, for example, Figure 2, thereby making this new kinetic method more convenient to use for others (and if so, does it verify the rate constants obtained by the programs we in part wrote and used initially)? Does a control experiment fully support our past back-extrapolation treatment of the initial pressure rise seen experimentally in the induction period and attributed to the volatile acetone solvent's vapor pressure? Can we show

(10) Note also that implicit in the kinetic treatment is the *approximation* that all Ir(0) surface atoms on the growing, and thus temporally different sizes, nanoclusters react at the same rate. This approximation (i) is fully consistent with the literature of olefin hydrogenation being a structure-insensitive reaction, (ii) is further supported by the direct monitoring of the Ir(0) formation by its cyclooctane evolution reaction (because the two methods yield the same rate constants within experimental error; this requires that there is not, as expected, a detectable particle size dependence *difference* between cyclohexene and cyclooctadiene hydrogenation), and (iii) in any event is a necessary approximation in these *first studies* because a range of different particle sizes is only now becoming available to see if this approximation holds in nanocluster catalysis. We note, however, that an obvious goal of future studies is to determine independently the particle-size effects in, especially, nanocluster-catalyzed structure-sensitive reactions, and then to see if the same particle-size effects can be deconvoluted out of kinetic curves analogous to those in Figures 2, 4, 5, and 6.

(11) Lyon, D. K.; Finke, R. G. *Inorg. Chem.* **1990**, *29*, 1787.
(12) Aiken, J. D., III; Finke, R. G.; *J. Am. Chem. Soc.* **1998**, *120*, 9545.
(13) Watzky, M. A.; Finke, R. G. *Chem. Mater.* **1997**, *9*, 3083.

that the pseudoelementary step method for following nanocluster growth works for other, more difficult and slower reactions[14] and with metals other than Ir (e.g., the Rh-catalyzed arene hydrogenations that we are investigating[15])? Can we show that a computer numerical integration kinetic simulation of the more detailed mechanism implied by Scheme 1, consisting of the first 50 or so truly elementary mechanistic steps, produces a sigmoidal curve as expected? If so, can such a simulated curve be fit by our $\mathbf{A} \rightarrow \mathbf{B}$, $\mathbf{A} + \mathbf{B} \rightarrow 2\mathbf{B}$ (rate constants k_1 and k_2) model, thereby offering further support for the mechanism in Scheme 1 and its implied more detailed version? (Or, if not, what needs to be added or changed in the minimalistic, Occam's Razor mechanism in Scheme 1?) And, finally, what else can we learn about the mechanism in Scheme 1 if we examine additional metals such as Ru(II) under H_2 and en route to its corresponding nanoclusters? It is exactly these previously unanswered questions that are experimentally investigated herein and in the order presented above.

Results and Discussion

Verification of the Kinetic Method and the H_2 Uptake Stoichiometry in Equation 1: Hydrogen Uptake of the Precatalyst in the Absence of Cyclohexene and in Propylene Carbonate Solvent. The new kinetic method presented herein uses the convenient but indirect means of cyclohexene hydrogenation activity to follow nanocluster growth. When possible, it is best to verify such indirect methods by direct techniques. We were able to do just that by following the reduction of the precatalyst **A** in the absence of substrate. The experiment was performed on a high-vacuum line with a high-precision pressure transducer capable of detecting ±0.1 Torr (i.e., ±0.002 psig) pressure changes—that is, a transducer 5 times more sensitive than our standard hydrogenation system for monitoring nanocluster formation via cyclohexene hydrogenation.[8] Initially, we attempted to use our standard solvent of acetone[5,8] to perform the desired H_2 uptake experiment. However, it was discovered using this more sensitive detector that, at least in the absence of the more readily hydrogenated cyclohexene, the $Ir(0)_n$ nanoclusters slowly hydrogenate the acetone solvent to form 2-propanol. (The formation of 2-propanol was verified by GLC and ^{1}H NMR, as shown in Figures G, H, and I of the Supporting Information.) Hence, acetone proved unsuitable for H_2 uptake experiments monitoring the reduction of **A** alone (but not for nanocluster studies followed by the much faster cyclohexene hydrogenation and where the net H_2 consumption due to solvent hydrogenation is negligible).

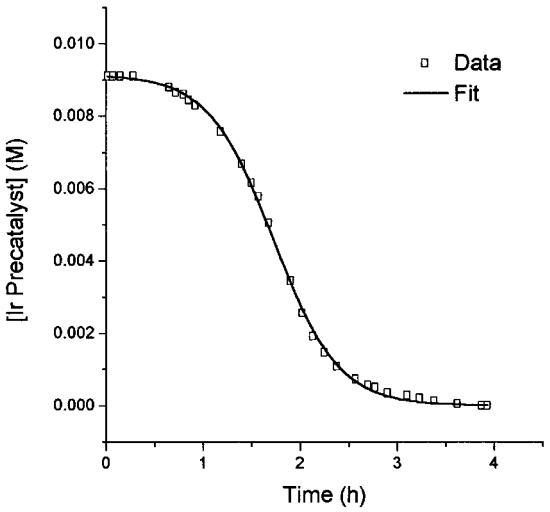

Figure 4. Plot of the loss of Ir precatalyst **A** (or, equivalently, by eq 1 the H_2 uptake) vs time due to the reduction of **A** by H_2 and in the absence of added cyclohexene. As shown, the sigmoidal curve is fit almost exactly by the identical analytic kinetic equations, corresponding to eqs 2a and 2b (vide supra), which were used in our earlier work to fit kinetic curves such as the one back in Figure 2.

A search for suitable solvents revealed that propylene carbonate is *not* hydrogenated under the conditions of the H_2 uptake experiments and even at the detection limits of the high-precision pressure transducer. Accordingly, the hydrogen uptake due to the reduction of $[Bu_4N]_5Na_3[(1,5\text{-COD})Ir{\cdot}P_2W_{15}Nb_3O_{62}]$, **A**, alone was followed vs time and to ±0.1 Torr in an experiment in which 0.103 g of **A** was dissolved in 2.0 mL of propylene carbonate at 22.5 °C and with an initial H_2 pressure of 263.3 Torr (5.091 psi). Note that these conditions are necessarily at a lower H_2 pressure, as well as a different solvent, in comparison to our 40 psig H_2 (≈52 psi at our mile-high altitude where atmospheric pressure is ≈640 Torr) and acetone "standard conditions" used in our previous kinetic studies employing the pseudoelementary step method.[8]

Despite the necessarily different reaction conditions, the resulting hydrogen uptake curve, Figure 4, still has the expected sigmoidal shape; the associated induction period is about 30 min and the complete reaction time is about 4 h. As Figure 4 also shows, the resultant H_2 uptake curve can be closely fit by the identical analytic kinetic equations used previously (eqs 2a and 2b).[8] Note that the curve in Figure 4 is now closely fit, even at the end of the reaction (cf. to the poorer fit in Figure 2 for this part of the curve), as it should be because there is no cyclohexene hydrogenation reporter reaction (no use of the pseudoelementary step concept) in the experiment recorded in Figure 4. The resultant rate constants under the specified conditions of propylene carbonate solvent, 22.5 °C and 5.091 psi H_2, are $k_1 = 0.017$ h^{-1} and $k_{2(\text{fit})} = 330$ M^{-1} h^{-1} (no correction has been made to $k_{2(\text{fit})}$ for the *net* 3.5/1.0 H_2/**A** stoichiometry, nor were any other stoichiometry or scaling factors applied—see the Supporting Information for details).[16] The main conclusion from the H_2-uptake kinetic experiments, then, is the unequivocal demonstration that the reduction of **A** occurs in an autocatalytic manner. This experiment, in

(14) (a) Arene hydrogenation is, like simple olefin hydrogenation, a so-called "structure-insensitive" (i.e., largely particle-size-insensitive—see ref 24 below) reaction. Eventually, it will be important to look at highly particle-size-sensitive, structure-sensitive reactions as well, as then the k_1(apparent) and k_2(appparent) will contain valuable information about that size sensitivity.

(15) Widegren, J. A.; Finke, R. G., unpublished results and experiments in progress. One such arene hydrogenation experiment has been reproduced in Figure J of the Supporting Information for the interested reader. In this experiment the Rh nanocluster precursor, $[Bu_4N]_5Na_3[(1,5\text{-COD})Rh{\cdot}P_2W_{15}Nb_3O_{62}]$, is reduced in the presence of the more difficult substrate benzene (experimental conditions: 50 °C, 40 psig H_2, and propylene carbonate solvent). A sigmoidal hydrogen uptake curve results, characteristic of the nucleation and autocatalytic surface growth mechanism as summarized in Scheme 1, one which could be fit to the usual analytic equations for the reactions in eqs 2a and 2b.

turn, provides strong support for the validity of our pseudoelementary step kinetic method as a viable means for following nanocluster growth using the cyclohexene hydrogenation activity indirect assay.

Also of interest from the H_2 uptake experiment is the net stoichiometry in comparison to the predicted 2.5/1.0 H_2/**A** stoichiometry given back in eq 1 in which the 1.0 additional equiv of H_2 has been subtracted for the established reduction of the $P_2W_{15}Nb_3O_{62}^{9-}$ polyoxoanion to its two electron reduced "heteropolyblue",[5,8] $P_2W_{15}Nb_3O_{62}^{9-} + H_2 \rightarrow P_2W_{15}Nb_3O_{62}^{11-} + 2H^+$. Experimentally, and as expected, 3.6 ± 0.4 equiv of hydrogen (i.e., 2.5 + 1.0 = 3.5 equiv) was consumed per equivalent of **A** in the experiment shown in Figure 4. Also, the expected 1.0 equiv of cyclooctane product evolved within experimental error (experimentally 1.2 ± 0.2 equiv), as confirmed by quantitative GLC for the experiment shown in Figure 4, verifying that part of eq 1 as well. As has been noted elsewhere, such quantitative studies of nanocluster formation reactions leading to complete equations, which include mass and charge balance, are unfortunately a rarity in all of the nanocluster formation literature.[2d] Such balanced equations are, however and of course, *a prerequisite* to meaningful mechanistic studies.

A Second Verification of the Kinetic Method and Its Implied Nanocluster Formation Mechanism in Figure 3: Nanocluster Size vs Time as Determined by TEM. Nanocluster growth can also be followed directly by monitoring nanocluster sizes by TEM throughout a nanocluster formation reaction[7,17]—a powerful, direct way to follow nanocluster growth, at least *in principle*. In practice, the usefulness of TEM for kinetic studies of nanocluster growth in real time is greatly restricted by the time required to prepare the sample and to obtain even a single data point. In addition, the intrinsic TEM error limits of ±2 Å for non-HR-TEM microscopes propagate to an experimental error approaching ±5 Å in our experience,[13] a distance equivalent to plus or minus an entire shell of Ir(0) metal atoms. In short, a size difference of >10 Å between two TEM "kinetic data points" is required to ensure that the sizes are experimentally distinguishable. Despite these drawbacks, we felt it was important to verify by TEM the predicted features of nucleation and autocatalytic growth in the mechanism in Scheme 1: that one expects not to be able to see the small (<10 Å) nanoclusters during the induction period,[18] that one expects relatively small nanoclusters to be visible directly following the induction period, and that one expects nanoclusters of increasing size as the reaction continues to completion.

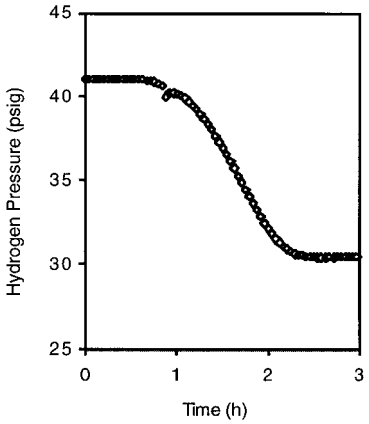

Figure 5. Hydrogen uptake curve in which a sample was removed for TEM analysis at 50 min. The temporary discontinuity in the curve at 50 min is due to the deliberate removal of a sample for TEM analysis. The first ≈30 min of the pressure data was back-extrapolated to remove the rise seen due to the acetone solvent's vapor pressure re-equilibration; see the section that follows on this topic for further details.

Two experiments were done to test these predictions. In the first experiment, a normal cyclohexene hydrogenation was started and then a sample was removed for TEM analysis after 30 min under hydrogen, a time which was still within, but approaching the end of, the induction period. No nanoclusters were seen by TEM in this sample, as expected, indicating that they are <10 Å or so in size. Because in the strictest sense this is a negative result, the control was done of confirming by TEM that in this particular reaction, after going to completion (20 h under hydrogen pressure), 23 (±4) Å nanoclusters were in fact formed (68 nanoclusters were measured; the reported error is ±1σ). It should also be noted that the hydrogen uptake curve (Figure C of the Supporting Information) for this experiment is very similar to that in Figure 5 above and exhibits the characteristic sigmoidal shape.

In the second experiment a normal cyclohexene hydrogenation experiment was started and a sample was removed for TEM analysis, but now after 50 min under hydrogen pressure and, hence, soon after the end of the induction period (Figure 5). The sample from the hydrogenation in Figure 5 contained 16 (±3) Å nanoclusters by TEM (180 nanoclusters were measured). Another TEM sample was then harvested *from this same hydrogenation experiment*, only now after 20 h of reaction under hydrogen, a time at which all of the precursor **A** is known to be converted into nanoclusters.[8] This 20-h sample contained 27 (±4) Å nanoclusters (207 nanoclusters were measured). In short, and as the new kinetic method and its resultant minimal mechanism (Figure 3) predict, the nanoclusters are <10, 16 (±3), and 27 (±4) Å as their sigmoidal formation curve, Figure 5, proceeds.

The Use of a Commercial Software Package for the Curve Fit Data Analysis. Previously, curve fitting of the H_2 pressure (or, equivalently, the cyclohexene concentration) vs time data was performed using a

(16) Because we know, in the presence of cyclohexene, that there is an olefin dependence to k_2, and probably also one to k_1 at lower olefin concentrations (see the top and bottom plots in Figure 6 elsewhere[8]), we expect a comparison of the above rate constants to those under our rather different "standard conditions"[8] (of acetone solvent, 1.65 M cyclohexene, 22 °C, and 40 psig of H_2) to reveal that the rate "constants" from these two different experiments are, simply, different (i.e., that k_1 and k_2 are really the pseudo-first- and pseudo-second-order rate constants k_1(obsd) and k_2(obsd)). In fact, a comparison of the rate constants from the curve fit in Figure 2 and where standard conditions were used, $k_1 = 0.010\ h^{-1}$ and $k_{2(\text{hydrogenation})\text{corrected}} = 3.6 \times 10^3\ M^{-1}\ h^{-1}$, to those given above confirms this prediction: they are different. (Note that $k_{2(\text{hydrogenation})\text{corrected}}$ is the value of k_2 after correcting for both the scaling and the stoichiometry factors—see the Supporting Information for details.)

(17) An excellent example of the use of TEM to follow nanocluster growth is provided by El-Sayed and co-workers 1998 paper.[4b]

(18) That is, one would not expect to see nanoclusters during the induction period as long as the size of the critical nucleus is too small to be visualized by TEM. For this system the critical nucleus size has been estimated at $\leq Ir(0)_{\sim 15}$,[8] which is too small to be seen by the microscope used in the present studies.

nonlinear regression subroutine (RLIN),[8] available in the IMSL Statistical Library, a subroutine that uses a modified Levenberg−Marquardt algorithm.[19] Calculations were done on an IBM/AIX workstation. A FORTRAN program was written that reads the list of input data points, defines the analytical expression to be used in the curve fit, asks for initial guesses of the variables (k_1 and k_2), and calls the appropriate RLIN subroutine.

Despite the full documentation of the above programs available elesewhere,[8] it seemed clear that the use of commercially available software that would run on a PC would aid the use of the new kinetic method detailed herein. Hence, we searched for generally available commercial packages that we could then test. As detailed below, the well-documented, commercial, nonlinear least-squares curve-fitting package Microcal Origin works well (we used version 3.5.4). Origin also uses a Levenberg−Marquardt algorithm to generate the nonlinear least-squares curve fit.

Two types of control experiments were done to ensure that the values of the Origin-determined k_1 and k_2 values are accurate. First, we calculated a "mock" set of data choosing $k_1 = 0.005$ h^{-1}, $k_2 = 1$ M^{-1} h^{-1}, and $[\mathbf{A}]_0 = 1.2$ M and using a time interval of 2.5 min (typical data as well as the same time interval that we use for a typical hydrogenation experiment). Fitting the first 110 data points in the calculated, mock data set, Origin found the same values (and produced the error bars) of $k_1 = 0.0050 \pm (6 \times 10^{-9})$ h^{-1} and $k_2 = 1.0 \pm (3 \times 10^{-7})$ M^{-1} h^{-1}, obviously identical to the input k_1 and k_2 values. This curve fit is available in the Supporting Information as Figure D.

Second, an experimental data set from a hydrogenation experiment starting with the precursor **A** was curve fit using our previous curve-fitting routine.[8] The resulting values of k_1 and k_2 were 0.0042 and 5.29, respectively. Next, the *exact same data points* were fit with Origin, resulting in k_1 and k_2 values of 0.0042 ± 0.0003 and 5.30 ± 0.06 (the error bars, again, are those determined by Origin). Again, the k_1 and k_2 values are identical within the error limits of the fit.

These results (i) identify a readily available, commercial curve-fitting package, (ii) validate the accuracy of that package for the present situation and curve fits, and (iii) also serve as a quantitative verification of the numbers from our previous curve-fitting program.

Control Experiments Examining Two Different Ways To Correct for Solvent Vapor Pressure and the Effect on the Resultant k_1 and k_2 Values from the Curve Fit. As detailed in the Experimental Section, the protocol for hydrogenation experiments with cyclohexene involves filling a Fischer−Porter (hereafter, F−P) pressure bottle with acetone solvent, cyclohexene, and the precatalyst **A**, all done in an N_2 atmosphere drybox. Then, the F−P bottle is removed from the drybox and attached to the hydrogenation line via Swagelok TFE-sealed quick connects (a full drawing of the apparatus is available elsewhere[5b]). Next, the N_2 in the F−P bottle is flushed out and replaced with 40 psig H_2. This is accomplished with 13−15 purge cycles (which consist of pressurizing the F−P bottle to ≈40 psig H_2 and then releasing the pressure from the vent valve) before the final pressurization to 40 psig H_2. During the purging cycles solvent vapor is also unavoidably swept out of the F−P bottle. Over the initial part of the hydrogenation experiment (≈0.5 h) the solvent vapor pressure returns to equilibrium, resulting in an initial *increase* in pressure being seen (as in Figure 6a). Our past treatment of this pressure increase[8,12,13,20] has been to simply back-extrapolate the data from the linear part of the induction period (and for induction periods longer than ≈0.5 h, vide infra), thereby removing this experimental artifact. This back-extrapolation was performed on the data shown in Figures 2 and 5, for example.

To test the validity of the back-extrapolation treatment of the data, we did a control experiment where

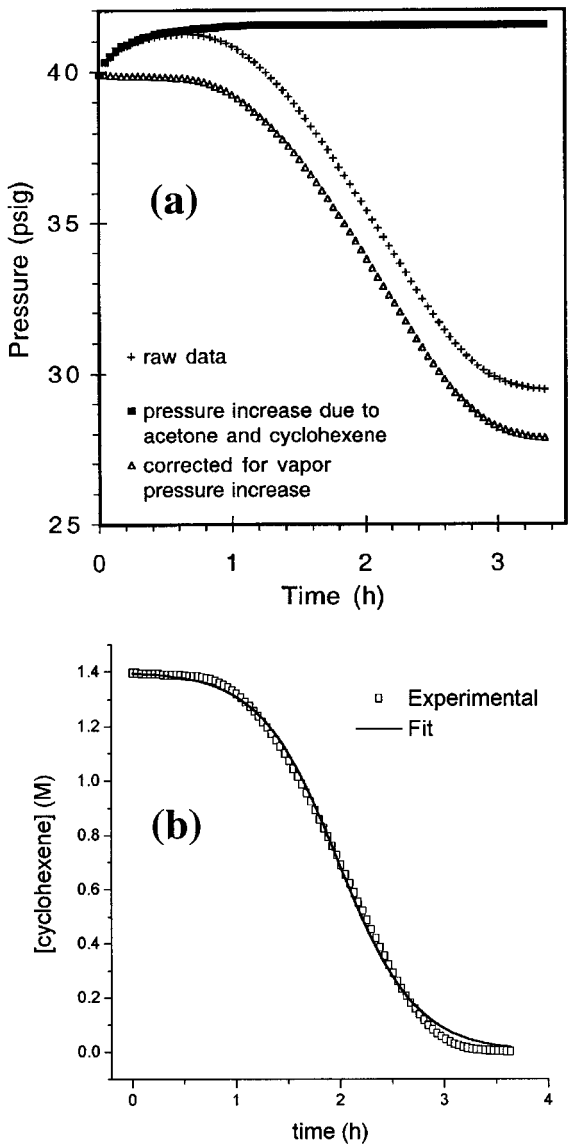

Figure 6. (a) Pressure vs time plot showing the raw data from the hydrogenation experiment shown in Figure 2 (note the initial increase in pressure due to solvent vapor pressure equilibration), the measured pressure vs time data for the vapor pressure increase of the acetone (plus its dissolved cyclohexene) following a standard cycle of purges in our apparatus, and the experimentally corrected hydrogen uptake curve. (b) The curve fit of experimentally corrected hydrogen uptake curve yields k_1 and k_2 values that are the same (within experimental error) as those for the back-extrapolated (normal treatment) data. A comparison of Figure 6b with Figure 2 shows the similarity of the two curves and the two curve fits.

(19) Press, W. H.; Flannery, B. P.; Teukolsky, S. A.; Vetterling, W. T. *Numerical Recipes*; Cambridge University: Cambridge, 1989.

we measured pressure vs time data for the vapor pressure increase of the acetone (plus its dissolved cyclohexene) following a standard cycle of purges. We then used that data to correct, point-by-point, the original data (i.e., before the back-extrapolation) from the cyclohexene hydrogenation experiment shown in Figure 2. Those curves are shown in Figure 6a. The experimentally corrected data were then curve-fit (Figure 6b). The k_1 and k_2 values for the experimental vapor pressure corrected data are $k_1 = 0.013\ h^{-1}$ and $k_{2(\text{hydrogenation})\text{corrected}} = 3.4 \times 10^3\ M^{-1}\ h^{-1}$, compared to $k_1 = 0.010\ h^{-1}$ and $k_{2(\text{hydrogenation})\text{corrected}} = 3.6 \times 10^3\ M^{-1}\ h^{-1}$ for the back-extrapolated data (normal treatment of the data).

An analysis of the data shows (i) that, indeed, it is the acetone solvent vapor pressure that causes most of the initial rise in pressure seen in the first ≈0.5 h of the induction period, (ii) that the experimentally corrected data may give a marginally better fit, but (iii) that the two treatments give k_1 and k_2 within experimental error (±15%) of each other, so (iv) that the more easily used, back-extrapolation method is what we recommend and what we will continue to use *so long as the induction period is ≥ ca. 0.5 h*. In addition, the data also show (v) that no such problem exists in cases where a less volatile solvent can be used (as in the use of propylene carbonate in Figure 4; note the lack of an initial pressure rise in that curve), but correspondingly, the use of a more volatile solvent, substrate, or product will require correction for their vapor pressure—that is, this is a subtle but important design feature in using the new method detailed herein. A derivation of the associated, simple pressure equations needed to understand exactly the underlying kinetics and mathematics of this vapor pressure correction to the kinetic experiments is provided in the Supporting Information.

Evidence for the New Method Being Applicable to Other Metals and Reactions: The Case of Rh(0) Nanoclusters in Olefin *and* Arene Hydrogenation. We have recently used the new kinetic and pseudoelementary step method herein to follow the formation of 40 ± 6 Å Rh(0) nanoclusters from hydrogenation of the precursor, $[Bu_4N]_5Na_3[(1,5\text{-COD})Rh\cdot P_2W_{15}Nb_3O_{62}]$, and in the presence of cyclohexene.[20] In an experiment directly analogous to that with the Ir congener, **A**, the Rh precursor yielded a sigmoidal hydrogen uptake curve, one closely fit by the kinetic equations (2a)−(2d), as shown in Figure 6 of ref 19. This shows that the method is applicable to at least Rh, Ir, and by implication, probably other transition metals as well. (See a later section for the application of the new method to Ru(0) nanocluster formation and the interesting findings that resulted.)

We wanted to see if we could change reactions, specifically to more difficult, slower reactions such as arene hydrogenation,[21] but then still use the new kinetic method to follow nanocluster formation.[22] Indeed, we have successfully done such an experiment using the Rh(0) nanocluster precursor, $[Bu_4N]_5Na_3[(1,5\text{-COD})Rh\cdot P_2W_{15}Nb_3O_{62}]$, and benzene as the substrate.[15] We have been able to use the new kinetic method herein to follow nanocluster formation for a second case of arene hydrogenation. Specifically, elsewhere[22] we have shown that the true catalysts, when beginning from the ion-pair precursor $[(C_8H_{17})_3NCH_3]^+[RhCl_4]^-$, are the Rh(0) nanoclusters that are shown to be present by TEM, *not* the discrete, monometallic ion pair as previously believed (see the references provided elsewhere[22]). The data demonstrate that the $[(C_8H_{17})_3NCH_3]^+[RhCl_4]^-$) precursor cannot be the catalyst to within the ≤±15% error limits of the $\mathbf{A} \rightarrow \mathbf{B}$, $\mathbf{A} + \mathbf{B} \rightarrow 2\mathbf{B}$ curve fits to the (in that case) mildly sigmoidal kinetic data[22]—that is, **A** can only be a catalyst precursor. The important point is that this is another example of the value of the new kinetic method and its ability to monitor nanocluster nucleation and growth.

Computer Kinetic (Numerical Integration) Modeling of Autocatalytic Surface Growth. To verify the general mechanism in Figure 3, we wanted to see if we could simulate, via numerical integration, the first 50 or so elementary steps implied by the pseudoelementary steps in Figure 3. In addition, we wanted to explicitly account for the range of nanoclusters of different sizes that are generated over the full course of the reaction, accounting explicitly and individually for the changing fraction of nanocluster surface atoms[23]—that is, to do this in a cluster-by-cluster way. The treatment of the (changing) fraction of surface atoms is important because only the surface atoms can participate in at least most common types of catalysis (i.e., and because we are not considering materials such as metal oxides where bulk oxide can participate in oxidation catalysis, for example). Specifically, we wanted to answer the questions: does a more "realistic" mechanism for nanocluster growth give the same type of sigmoidal olefin hydrogenation curve as predicted by eqs 2a−2d and as seen in Figures 2, 5, 6, and 8? If so, can that curve be fit by the pseudoelementary step model of eqs 2a−2d? Computer numerical integration kinetic modeling was used to answer these questions.

The kinetic model is shown in Scheme 2. The model first describes a $H_{2(gas)}$ to $H_{2(soln)}$ equilibrium. Then, the nucleation [$\mathbf{A} \rightarrow M(0)_1$] and growth [$\mathbf{A} + M(0)_1 \rightarrow M(0)_2$ through $\mathbf{A} + M(0)_{44} \rightarrow M(0)_{45}$] steps follow. Last, the alkene hydrogenation steps are shown. The rate constants and initial concentrations used for the kinetic model were made to correspond to a standard hydrogenation experiment as much as possible; see the Experimental Section for a detailed discussion. Note that the rate constants in Scheme 2 are distinguished from other rate constants in the text by the addition of

(20) Aiken, J. D., III; Finke, R. G. *Chem. Mater.* **1999**, *11*, 1035.

(21) A few lead references on arene hydrogenation include the following: (a) Collman, J. P.; Hegedus, L. S.; Norton, J. R.; Finke, R. G. *Principles and Applications of Organotransition Metal Chemistry*; University Science Books: Mill Valley, CA, 1987; pp 549−556. (b) Linn, D. E., Jr; Halpern, J. *J. Am. Chem. Soc.* **1987**, *109*, 2969. (c) Rothwell, I. P. *Chem. Commun.* **1997**, 1331. (d) Gao, H.; Angelici, R. J. *J. Am. Chem. Soc.* **1997**, *119*, 6937. (e) Ahn, H.; Marks, T. J. *J. Am. Chem. Soc.* **1998**, *120*, 13533. (f) Adams, C. J.; Earle, M. J.; Seddon, K. R. *Chem. Commun.* **1999**, 1043.

(22) Weddle, K. S.; Aiken, J. D., III; Finke, R. G. *J. Am. Chem. Soc.* **1998**, *120*, 5653.

(23) For experimental kinetic data, the changing fraction of surface atoms throughout a nanocluster formation reaction has been treated for the first time, and in a quantitative but average way, using the "scaling factor" described originally elsewhere[8] as well as in the Supporting Information accompanying the present paper. For example, $k_{2(\text{hydrogenation})\text{corrected}} = k_{2(\text{hydrogenation})}/0.8$ and (in the Supporting Information) $k_{2(\text{GLC})\text{corrected}} = k_{2(\text{GLC})}/0.7$. Note that in footnote 38b elsewhere[8] there is a typographical error in both this latter equation (it was inverted) and in the scaling factor (the previous 0.51 is in error).

Scheme 2. Kinetic Model Used To Account for the Production of Nanoclusters of Different Sizes and for the Effects of Surface Area (Time Units in This Scheme Are in Hours and the Concentration Units Are in Molarity)

$H_{2(gas)} \rightarrow H_{2(soln)}$	$k_f' = 1 \times 10^9$
$H_{2(soln)} \rightarrow H_{2(gas)}$	$k_r' = 4 \times 10^{11}$
$\mathbf{A} \rightarrow M(0)_1$	$k_1' = 0.002$
$\mathbf{A} + M(0)_1 \rightarrow M(0)_2$	$k_2' = 200$
$\mathbf{A} + M(0)_2 \rightarrow M(0)_3$	$k_3' = 383$
$\mathbf{A} + M(0)_3 \rightarrow M(0)_4$	$k_4' = 567$
•	•
•	•
•	•
$\mathbf{A} + M(0)_{44} \rightarrow M(0)_{45}$	$k_{45}' = 6829$
$M(0)_1 + \text{alkene} + H_{2(soln)} \rightarrow M(0)_1 + \text{alkane}$	$k_{46}' = 4.00 \times 10^5$
$M(0)_2 + \text{alkene} + H_{2(soln)} \rightarrow M(0)_2 + \text{alkane}$	$k_{47}' = 7.67 \times 10^5$
$M(0)_3 + \text{alkene} + H_{2(soln)} \rightarrow M(0)_3 + \text{alkane}$	$k_{48}' = 11.3 \times 10^5$
•	•
•	•
•	•
$M(0)_{45} + \text{alkene} + H_{2(soln)} \rightarrow M(0)_{45} + \text{alkane}$	$k_{90}' = 139 \times 10^5$

a "prime", for example, k_1', k_2', and so on. The kinetic model in Scheme 2 assumes that the rate of olefin hydrogenation and the rate of reaction of **A** with the growing nanoclusters are structure insensitive[24] (i.e., that there is no particle size dependence and every surface atom is assumed to have equal catalytic activity). The model also assumes that the nanoclusters grow in an "ideal" manner where each $M(0)_x$ corresponds to a single species[25] and where each shell of atoms becomes complete before growth occurs on the next shell. Nanocluster agglomeration is not accounted for in this model. The changing fraction of nanocluster surface atoms is explicitly taken into account by the choice of the rate constants $k_2'-k_{90}'$; full details are available in the Supporting Information. The nanoclusters were grown computationally to a maximum size of $M(0)_{45}$ because this represents the limit of the kinetic modeling software employed—MacKinetics version 0.9.1b, which has a limit of 50 chemical species. The actual kinetic scheme, as was typed into the MacKinetics program, is available in the Supporting Information.

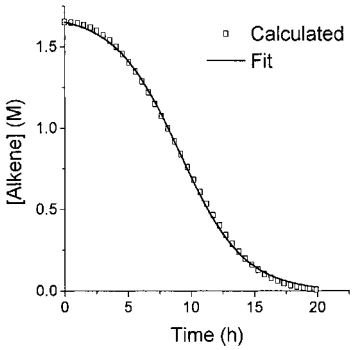

Figure 7. Results of the kinetic model showing that a sigmoidal curve is indeed produced. The "calculated" points from the kinetic model produce a curve that is closely fit by the identical analytic kinetic equations used to analyze the experimental hydrogenation curves.

The results of this kinetic model are shown in Figure 7. Note that *the kinetic model does indeed produce a sigmoidal curve*. Furthermore, the curve produced *is closely fit (Figure 7) by the identical analytic kinetic equations used to analyze the experimental hydrogenation curves*. Hence, this more detailed mechanism for nanocluster growth does indeed give the same type of sigmoidal olefin hydrogenation curve as predicted by eqs 2a−2d and as seen experimentally in Figure 2. The values of the rate constants yielded by the curve fit in Figure 7 are $k_1 = 0.027\ h^{-1}$ and $k_{2(\text{hydrogenation})\text{corrected}} = 300\ M^{-1}\ h^{-1}$ ($k_{2(\text{hydrogenation})\text{corrected}}$ is the value of k_2 after correcting for both the scaling and the stoichiometry factors—see the Supporting Information for details). One might be tempted to compare the values of k_1 and $k_{2(\text{hydrogenation})\text{corrected}}$ to the individual rate constants k_1' and k_2' from Scheme 2. However, k_1 and $k_{2(\text{hydrogenation})\text{corrected}}$ are not elementary step rate constants and are not solely dependent on values chosen for k_1' and k_2'. For example, k_1 and $k_{2(\text{hydrogenation})\text{corrected}}$ both become larger as rate constant values for the olefin hydrogenation steps ($k_{46}'-k_{90}'$) are increased. As a final note, additional simulations demonstrate that a sigmoidal olefin hydrogenation curve is also produced if one requires a "critical nucleus" to form before olefin hydrogenation activity can begin (see Figure E of the Supporting Information for the case where the nanoclusters were required to be $\geq M(0)_{13}$ before they became active olefin hydrogenation catalysts). On the basis of the fraction of cyclooctane evolution vs time in our previous work, a critical nucleus size of $\leq$15Ir(0) atoms has been estimated.[8]

The Discovery of the Importance of Heterolytic Hydrogenation Activation—and the Need To Add Base To Initiate Nanocluster Formation—for Cationic Metals Such as Ru(II) That Do Not Undergo Ready *cis*-Oxidative Addition of H_2. As part of our extension to other metals, we investigated the hydrogen uptake curves of a Ru(II) system based on the precatalyst $[Bu_4N][Ru(1,5\text{-}COD)(CH_3CN)(P_3O_9)]$, with cyclohexene present and using the pseudoelementary step reporter method to monitor nanocluster formation. Not unexpectedly, we found that, under H_2 alone, nanoclusters did not form (Figure 8a), even at times 5−10-fold longer than needed to form the Rh or Ir nanoclusters.

(24) Lead references and further discussion of structure-sensitive or -insensitive reactions are available in footnote 52 elsewhere.[5b] (b) Note, however, that ethylene hydrogenation on $Pt(0)_n$ particles supported on SiO_2 is a stucture-insensitive reaction only to an *apparent* factor of ≤3; see Figure 9 p 110 of Che, M.; Bennett, C. O. *Adv. Catal.* **1989**, *36*, 55−172. Note that we say apparent because one cannot rule out, on the basis of only the data in Figure 9 of the Che and Bennett paper, a SiO_2 effect on the hydrogenation rate that is somehow also a function of the $Pt(0)_n$ particle size (i.e., rather than an intrinsic rate effect due solely to the metal particle size and completely independent of the SiO_2). This example illustrates why we believe nanoclusters will prove valuable in testing such often cited, but still too phenomenology-based, mechanistic concepts of heterogeneous catalysis.

(25) In reality a large number of nanocluster geometries are possible for each $M(0)_x$, with surface irregularities (roughness; facets) and a more fluidlike surface structure probably being much more common than is generally recognized: (a) Uppenbrink, J.; Wales, D. J. *J. Chem. Phys.* **1992**, *96*, 8520. (b) Doye, J. P. K.; Wales, D. J. *New J. Chem.* **1998**, 773. (c) Soler, J. M.; Beltrán, M. R.; Michaelian, K.; Garzón, I. L.; Ordejón, P.; Sánchez-Portal, D.; Artacho E. *Phys. Rev. B* **2000**, *61*, 5771. (d) Lewis, L. J.; Jensen, P.; Barrat, J.-L. *Phys. Rev. B* **1997**, *56*, 2248. (e) Dassenoy, F.; Casanove, M. J.; Lecante, P.; Verelst, M.; Snoeck, E.; Mosset, A.; Ely, T. O.; Amiens, C.; Chaudret, B. *J. Chem. Phys.* **2000**, *112*, 8137. (f) See the quote on p 719 elsewhere[1b] that calculations "have shown that there are many metastable (structural) configurations in a 0.1 eV range above the equilibrium state, and that their number increases significantly with the cluster size". (g) For Si_n nanoclusters: Ballone, P.; Andreoni, W.; Car, R.; Parrinello, M. *Phys. Rev. Lett.* **1988**, *60*, 271.

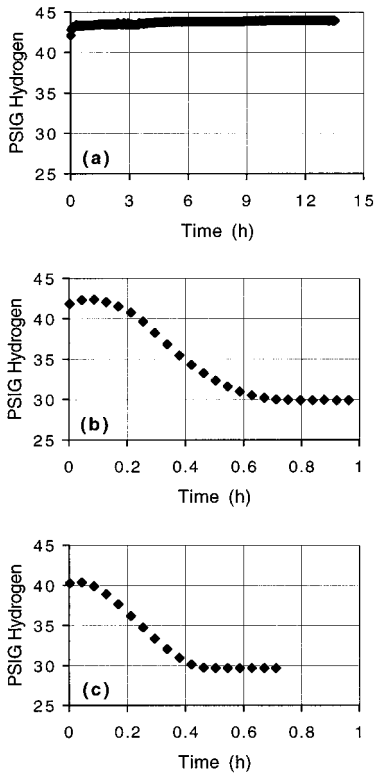

Figure 8. Hydrogen uptake curves produced by the Ru(II) precatalyst $[Bu_4N][Ru(1,5\text{-}COD)(CH_3CN)(P_3O_9)]$ in (a) the absence of base, with (b) 1.0 equiv of $Bu_4N^+OH^-$ added, and with (c) 2.0 equiv of $Bu_4N^+OH^-$ added. Not unexpectedly, we found that, in the absence of added base (i.e., under H_2 alone), nanoclusters did not form, even after >13 h. The addition of 1.0 equiv of $Bu_4N^+OH^-$ does indeed "turn on" the formation of nanoclusters, shortening the induction period for nanocluster formation to about 10 min. The addition of a second equivalent of $Bu_4N^+OH^-$ shortens the induction period by an additional factor of 2 to about 5 min.

We reasoned that oxidative-addition activation of H_2 by the present Ru(II) precursor to yield $Ru^{IV}(H)_2$ is energetically prohibitive. We further reasoned that heterolytic hydrogen activation[26] is required to initiate the formation of Ru(0) nanoclusters; hence, the addition of a base is crucial as can be seen by the general stoichiometry for heterolytic hydrogen activation, eq 3. Note that depending upon the strength of the base and the pK_a of the resultant M−H, the required stoichiometry can be between 1 equiv of base (eq 3a) and 2 equiv of base (eqs 3b and 3c). As Figure 8b shows, the addition

$$M^{n+} + H{-}H + :B \longrightarrow M{-}H^{n-1} + BH^+ \quad (3a)$$

$$M{-}H^{n-1} + :B \longrightarrow :M^{n-2} + BH^+ \quad (3b)$$

$$\text{SUM:}\quad M^{n+} + H{-}H + 2:B \longrightarrow :M^{n-2} + 2\,BH^+ \quad (3c)$$

of 1.0 equiv of tetrabutylammonium hydroxide ($Bu_4N^+OH^-$) does indeed "turn on" the formation of nanoclusters from this divalent metal precursor: the induction period for nanocluster formation (as monitored by their catalytic activity using the methodology reported herein) drops from >13 h to about 10 min for the Ru(II) precursor, a rate increase of >78-fold. Figure 8c shows that the addition of a second equivalent of strong base shortens the induction period by (only) an additional factor of 2 to about 5 min.

A search of the heterolytic hydrogen activation literature[26] revealed (i) that the key requirements for heterolytic hydrogenation are a metal whose oxidation state is high enough that further oxidation is unfavorable, an available coordination site and a way to stabilize the released proton (i.e, the presence of a base), especially in nonaqueous solvents, (ii) that amines, carboxylates, alkoxides, and hydroxides are commonly used bases (the base can also be an internal M−R that undergoes a four-centered reaction with H_2 that is a second version of heterolytic hydrogen activation[26a]), and (iii) that it is difficult to distinguish mechanistically true heterolytic hydrogenation activation from the two-step sequence of oxidative addition followed by deprotonation of the metal hydride by the added base. Nevertheless, (iv) practically speaking the metals that undergo the net reaction stoichiometry of eq 3, *where the presence of base may generally be required to initiate nanocluster formation, include Pd(II), Pt(IV), Ru(II), Ru(III), Rh(III), Ir(III), Ag(I), Au(III), Cu(I), and Cu(II).* Note that the added base is required only for the *nucleation step* back in Scheme 1; once $M(0)_n$ nanoclusters of the critical nucleus size (or larger) are formed, they can then activate H_2 by *cis*-oxidative addition on the $M(0)_n$ surface and then grow by the autocatalytic surface-growth mechanism (Scheme 1). In fact, we recommend that the use of coordinating vs noncoordinating bases (e.g., a prototype noncoordinating base being Proton Sponge, 1,8-bis(dimethylamino)naphthalene) be a design consideration in the synthesis of nanoclusters of the above metals and under H_2, along with thoughts about whether more than 1 equiv of a coordinating base should be used (excess base being a good ligand and, hence, a poison for nanocluster surface sites, thereby inhibiting subsequent surface-based, *autocatalytic* growth.

We wondered whether literature nanocluster formation reactions under hydrogen beginning with Pd(II),[27−36] Pt(IV),[28,35,36,38,39] Ru(III),[35,40−42] Rh(III),[35,36,40,43−45,41,46,42] Ag(I),[28,29] Au(III),[28,29] Cu(II),[47,29] and Ir(III)[35,36] require

(26) (a) Collman, J. P.; Hegedus, L. S.; Norton, J. R.; Finke, R. G. *Principles and Applications of Organotransition Metal Chemistry*; University Science Books: Mill Valley, CA, 1987; pp 291−293. (b) Brothers, P. J. *Prog. Inorg. Chem.* **1981**, *28*, 1.

(27) Bönnemann, H.; Brinkmann, R.; Neiteler, P. *Appl. Organomet. Chem.* **1994**, *8*, 361.
(28) Clay, R. T.; Cohen, R. E. *Supramol. Sci.* **1995**, *2*, 183.
(29) Clay, R. T.; Cohen, R. E. *Supramol. Sci.* **1997**, *4*, 113.
(30) Fukuoka, A.; Sato, A.; Kodama, K.-Y.; Hirano, M.; Komiya, S. *Inorg. Chim. Acta* **1999**, *294*, 266.
(31) Schmid, G.; Harms, M.; Malm, J.-O.; Bovin, J.-O.; Ruitenbeck, J. v.; Zandbergen, H. W.; Fu, W. T. *J. Am. Chem. Soc.* **1993**, *115*, 2046.
(32) Vargaftik, M. N.; Zagorodnikov, V. P.; Stolarov, I. P.; Moiseev, I. I.; Kochubey, D. I.; Likholobov, V. A.; Chuvilin, A. L.; Zamaraev, K. I. *J. Mol. Catal.* **1989**, *53*, 315.
(33) Ciebien, J. F.; Cohen, R. E.; Duran, A. *Supramol. Sci.* **1998**, *5*, 31.
(34) Henglein, A. *J. Phys. Chem. B* **2000**, *104*, 6683.
(35) Landré, P. D.; Richard, D.; Draye, M.; Gallezot, P.; Lemaire, M. *J. Catal.* **1994**, *147*, 214.
(36) Boutonnet, M.; Kizling, J.; Stenius, P.; Maire, G. *Colloids Surf.* **1982**, *5*, 209.
(37) Toshima, N.; Takahashi, T.; Hirai, H. *Chem. Lett.* **1985**, 1245.
(38) Meguro, K.; Torizuka, M.; Esumi, K. *Bull. Chem. Soc. Jpn.* **1988**, *61*, 341.
(39) Toshima, N.; Takahashi, T. *Bull. Chem. Soc. Jpn.* **1992**, *65*, 400.

the presence of added base. That is, has this very fundamental key to producing nanoclusters from metals in higher oxidation states been missed previously as we suspected? Has the availability of our new method for easily monitoring nanocluster growth allowed us to discover a key to the rational synthesis of nanoclusters from electrophilic metals placed under H_2?

In fact, a search of the nanocluster and colloid literature reveals that M(0) nanoclusters prepared from metal salts or organometallic complexes of Pd(II), Pt(IV), Ru(III), Rh(III), Ag(I), Au(III), Cu(II), and Ir(III) with hydrogen as the reductant have commonly been prepared *in the presence of a base*. Bases such as alkylammines,[35,40−46] ammonia,[47] carboxylates,[27−29,31,32,34] and alkoxides[30] have been used. It is also common for the base to be coordinated to the metal (e.g., palladium(II)acetate is often used as a precursor to Pd(0) nanoclusters when hydrogen is used as the reductant[27,31,32]). Interestingly, there appears to be only one prior example in the nanocluster synthesis literature where the necessity of the base was recognized.[47] However, even in that work the possible generality of heterolytic hydrogen activation for nanocluster formation from electrophilic metals went unrecognized.[47] Importantly, there are cases where nanocluster formation is not seen, even when forcing conditions were tried, *but in the absence of base*.[48]

The lack of an easily applied method to follow nanocluster formation reactions in real time is probably what has delayed the discovery of heterolytic hydrogen activation in nanocluster formation until now. The present first recognition of the importance of heterolytic hydrogen activation in nanocluster nucleation reactions from higher valent metals placed under H_2, a discovery made possible by the new kinetic method presented in this paper, promises to be valuable insight for the rational synthesis of nanoclusters of metals such as Pd(II), Pt(IV), Ru(III), Rh(III), Ag(I), Au(III), Cu(II), and Ir(III).

Summary and Conclusions

To summarize, our new indirect but continuous, easy, quantitative, and powerful way to monitor transition-metal nanocluster formation under H_2 has been developed in greater detail and with an eye toward making it as easy as possible for other researchers to use. The method has been further investigated, improved, and documented: (i) by showing that direct monitoring of the nanocluster formation (by following the H_2 uptake due only to the nanocluster formation reaction, or by following nanocluster size by TEM) gives the predicted sigmoidal kinetic curve and nanocluster size dependencies vs time, respectively; (ii) by finding and testing for accuracy a commercial nonlinear least-squares curve-fitting package that should be readily available and easily implemented by others; (iii) by doing key control experiments to document how to handle volatile solvents or substrates; (iv) by showing that nanocluster formation can be successfully monitored for other metals and more difficult reactions, such as Rh-catalyzed arene hydrogenation; (v) by showing that computer kinetic simulations provide strong support for the more detailed mechanism implied by the Occam's razor mechanism in Scheme 1; and significantly (vi) by discovering, via the new kinetic method, heterolytic hydrogen activation with its requirement for ≥ 1 equiv of added base in the nanocluster nucleation steps of certain higher valent, electrophilic metals. This last finding adds eqs 3a−3c as an important variant in the nucleation steps back in the generalized mechanism in Scheme 1. In fact, heterolytic hydrogen activation can now be added to the list of other findings noted in the Introduction and that were discovered using the new kinetic methodology presented herein (i.e., implications for shape and size control via the living metal polymer concept;[13] the first mechanistic explanation for why magic number sized nanoclusters tend to form;[13] how to make onionskin geometry bi-, tri-, and higher multimetallic nanoclusters,[13] and now the importance of heterolytic hydrogen activation in the formation of nanoclusters under H_2 from higher valent M^{n+} precursors).

It is our hope that the present studies, plus our earlier work,[5,8,12,13,20,22] will allow others to use this new methodology to monitor their nanocluster formation reactions under reductive conditions. We are certainly continuing to use this methodology to monitor a wide range of nanocluster formation reactions in our own laboratories. Also planned are additional studies to see if the methods herein can be extended to a range of other reductants besides H_2, to a range of other metals whose nanoclusters are of interest, and to the important cases of particle-size-sensitive (i.e., "structure-sensitive") reactions.

Experimental Section

Materials. Acetone was purchased from Burdick & Jackson (water content < 0.2%) and stored in a vacuum atmosphere drybox. The source, purity, and water content of the acetone or other solvents are known to be important in the nanocluster

(40) Bönnemann, H.; Braun, G.; Brijoux, W.; Brinkmann, R.; Schulze Tilling, A.; Seevogel, K.; Siepen, K. *J. Organomet. Chem.* **1996**, *520*, 143.
(41) Fache, F.; Lehuede, S.; Lemaire, M. *Tetrahedron Lett.* **1995**, *36*, 885.
(42) James, B. R.; Wang, Y.; Alexander, C. S.; Hu, T. Q. *Can. Chem. Ind.* **1998**, *75*, 233.
(43) Yonezawa, T.; Tominaga, T.; Richard, D. *J. Chem. Soc., Dalton Trans.* **1996**, 783.
(44) Landré, P. D.; Lemaire, M.; Richard, D.; Gallezot, P. *J. Mol. Catal.* **1993**, *78*, 257.
(45) Nasar, K.; Fache, F.; Lemaire, M.; Béziat, J.-C.; Besson, M.; Gallezot, P. *J. Mol. Catal.* **1994**, *87*, 107.
(46) Weddle, K. S.; Aiken, J. D., III.; Finke, R. G. *J. Am. Chem. Soc.* **1998**, *120*, 5653.
(47) Kanda, S.; Kori, T.; Kida, S. *J. Solid State Chem.* **1994**, *108*, 299.
(48) An illustrative example comes from a 1994 paper.[27] Those workers attempted to make Pd(0) colloids from four similar Pd(II) precursors ($[N(octyl)_4]_2PdBr_4$, $[N(octyl)_4]_2PdCl_4$, $[N(octyl)_4]_2PdCl_2Br_2$, and $Pd(acetate)_2/[N(dodecyl)_4]Br$) and using H_2 as the reductant. The $[N(octyl)_4]_2PdBr_4$ could not be reduced (even under 50 bar H_2), $[N(octyl)_4]_2PdCl_4$ gave only a precipitate, $[N(octyl)_4]_2PdCl_2Br_2$ was reduced very slowly (after 14 days!) under 1 atm of H_2, yet $Pd(acetate)_2/[N(dodecyl)_4]Br$ was reduced in 16 h (a factor of >21 faster) under the same conditions.[27] Those workers correctly made the phenomenological conclusion that "the anion of the palladium salt is crucial for the success of the colloid synthesis",[27] but failed to have any fundamental insights as to why the anion is key. We can now offer a very likely if not compelling hypothesis that the presence of a base (acetate) is allowing the $Pd(acetate)_2/[N(dodecyl)_4]Br$ precursor to be reduced *initially* by a heterolytic hydrogen activation pathway. None of the other three precursors contained a base and therefore have a large kinetic barrier to the nucleation of their nanocluster formation reactions.

Experimental Section

formation reaction.[5,8] Cyclohexene (Aldrich, 99%) was purified by distillation from Na under argon and stored in the drybox. Propylene carbonate (Aldrich, 99.7%, anhydrous, packaged under N_2) was transferred into the drybox and used as received. Ethanol (95 vol %) was prepared by mixing 19 mL of anhydrous ethanol (Pharmco) with 1.0 mL of "nanopure" water (distilled water filtered through a Barnstead filtration system). Tetrabutylammonium hydroxide ($Bu_4N^+OH^-$) was purchased from Aldrich as a 1.0 M aqueous solution. A 0.5 M solution of $Bu_4N^+OH^-$ was made by diluting the 1.0 M solution with nanopure water. The iridium nanocluster precursor complex $[Bu_4N]_5Na_3[(1,5\text{-COD})Ir{\cdot}P_2W_{15}Nb_3O_{62}]$ (**A**)[6a] was prepared from $[Bu_4N]_9[P_2W_{15}Nb_3O_{62}]$ made by our most recent method[6b] [and using $NbCl_5$ as the Nb source, as detailed in footnote 20 of ref 6b (this footnote has a typographical error—a 0.5% solution of H_2O_2 is used, *not* a 5% solution)] and was stored in the drybox. The ruthenium precatalyst $[Bu_4N][Ru(1,5\text{-COD})(CH_3CN)(P_3O_9)]$ was prepared following literature procedures[49] and was stored in the drybox.

Hydrogenations. These were generally done as before; see the Experimental Section elsewhere[8] under the identical heading, "Hydrogenations". Briefly, in the drybox 20 ± 1 mg of **A** was dissolved in 2.5 mL of acetone and 0.5 mL of cyclohexene. This bright yellow solution was transferred into a new 22 × 175 mm Pyrex culture tube containing a $^5/_8 \times {}^5/_{16}$ in. stir bar. The culture tube was placed in a Fischer−Porter (F−P) pressure bottle modified with Swagelock TFE-sealed Quick-Connects. The F−P bottle was then sealed, brought out of the drybox, placed in a 22.0 °C temperature controlled water bath, and connected to a H_2 line via the Quick-Connects. The F−P bottle was then purged 15 times (waiting 15 s between purges) with 40 psig H_2. Following the purges, the F−P bottle was pressurized to 40 (±1) psig H_2. During the purging (and during the hydrogenation reaction) the reaction solution was vortex-stirred. Five minutes after the beginning of the purges was designated $t = 0$, and at this time data collection was initiated using an Omega PX-621 pressure transducer interfaced to a PC.

Hydrogen Uptake from the Precatalyst Alone (i.e., in the Absence of Cyclohexene). A drawing of the gas uptake apparatus used for this experiment is given in the Supporting Information. It consists of the following major pieces: a high-vacuum line ($\leq 10^{-4}$ Torr, as continuously monitored by a Varian 524-2 cold cathode gauge); a 50-mL Pyrex reaction flask of known volume; and a MKS Type 122A Baratron pressure transducer (+999 Torr maximum pressure; ±0.1 Torr), also of known volume.

While in a nitrogen atmosphere drybox, **A** (103.4 mg, 1.82×10^{-5} mol) was weighed into a two-dram vial. Propylene carbonate (2.0 mL) was then added via a gastight syringe to yield a dark, orange-amber, homogeneous solution. This solution was transferred via a disposable polyethylene pipet into the reaction flask (which also contained a 1 × 3 mm Teflon-coated magnetic stir bar). The flask was sealed, brought out of the drybox, and attached to the gas-uptake apparatus. Next, the reaction solution was degassed (to $<10^{-4}$ Torr) via three freeze−pump−thaw cycles at liquid nitrogen temperature. Upon final thawing, the reaction solution was warmed to room temperature (22.5 °C), vortex stirring was initiated, and hydrogen was introduced into the vacuum line. Then, the part of the vacuum line containing the reaction flask and the pressure transducer was isolated at an initial pressure of 263.0 Torr H_2. Hydrogen uptake was observed after an induction period of approximately 30 min. No further hydrogen uptake was observed after 4 h of reaction, at which time the pressure had decreased to 249.9 Torr H_2 (which corresponds to an uptake of 3.6 ± 0.4 equiv of hydrogen/mol of **A**). During the course of the reaction the solution became a dark blue-black color as expected for the precedented formation of the 2 e^- reduced, heteropolyblue-blue, $H_2[P_2W^{VI}_{13}W^{V}_{2}Nb_3O_{62}]^{9-}$.[5] Quantitative GLC confirmed that 1.2 ± 0.2 equiv of cyclooctane had evolved during the reaction, indicating complete reduction of **A**.

TEM Size Determination of the Ir(0) Nanoclusters vs the Extent of Their Formation Reaction. These experiments were started as "Standard Conditions" cyclohexene hydrogenations (see the section entitled "Hydrogenations"). At a predetermined time during the hydrogenation reaction (and as shown by the discontinuity in the data in Figure 5), a sample was withdrawn from the F−P bottle by first opening the F−P bottle up to the H_2 line and then opening the top (purge) valve on the F−P bottle. This arrangement provided a constant flow of H_2 out of the F−P bottle and thus protected the contents from O_2. An 18-in. stainless steel needle (attached to a 1-mL plastic syringe) was threaded down into the F−P bottle and a 0.3-mL sample of the reaction solution was removed. (The needle and syringe were both purged with H_2 prior to insertion into the F−P bottle.) The sample was syringed into a disposable one-dram glass vial, which was capped immediately. The vent valve on the F−P bottle was then closed, the F−P bottle was repressurized to the pressure present just before the pressure release (see the discontinuity point in Figure 5), and the hydrogenation reaction was allowed to continue. A disposable syringe needle was then pushed through the cap of the sample vial before placing the sample into the antechamber of the drybox. After evacuation of the antechamber, the sample (which was dry by this time) was brought into the drybox. The entire sampling procedure took about 2 min, including repressurizing the F−P bottle and placing the sample in the antechamber.

After 20 h under hydrogen the hydrogenation reaction was stopped and TEM samples were prepared from the final reaction solution as described in a section available elsewhere[8] labeled "(G) Transmission Electron Microscopy (TEM)". Briefly, the F−P bottle was brought back into the drybox and the reaction solution (a dark suspension) was transferred into a glass vial. The polyoxoanion-stabilized nanoclusters were allowed to separate before the colorless supernatant was removed with a pipet. The precipitate was then dried and sent as a solid to the University of Oregon for TEM analyses, performed there as before[8] by Dr. Eric Schabtach. The samples removed during the hydrogenation reaction (taken at 30 and 50 min in separate experiments) were also sent as solids to the University of Oregon for TEM.

The Use of a Commercial Software Package for the Curve-Fit Data Analysis. When making initial guesses in Origin for the values of k_1 and k_2, it was found that for the subroutine to converge, one must guess a value of k_1 that is within about 4 orders of magnitude of the "real" value. Initial guesses for k_2 are simpler to make because the subroutine will almost always converge if the value guessed is *smaller* than the real value, even if the guess is 20−30 orders of magnitude smaller! However, guessing values of k_2 that are as little as 5−10 times larger than the real value can cause failure to converge. One advantage of using Origin is that it is not necessary to pick a wide range of empirical initial guesses to avoid local minima because one can watch as the curve fit approaches the data (i.e., Origin displays and continually updates its calculated curve fit for comparison to the actual data).

As with all numerical integration methods, it is important to choose the right units for the time data when curve fitting in Origin. If the induction period is a big number in whatever time units chosen, then the value of k_1 is small with dimensions of those units^{-1}. As the value of k_1 becomes very small, the relative error in the curve fit generally becomes larger (plus getting the program to converge if k_1 is very small seems to be more difficult). Hence, we recommend picking the time units (s, h, days, etc.) so that the induction period is about 10 of those units or less.

Computer Kinetic Modeling (Numerical Integration) of Autocatalytic Surface Growth. The initial concentrations used for the kinetic model (Scheme 2) were made to correspond to a standard hydrogenation experiment as much as possible. The initial concentrations of precatalyst and alkene used for the model were $[\mathbf{A}]_0 = 0.0012$ M and $[\text{alkene}]_0 = 1.65$

(49) Attanasio, D.; Bachechi, F.; Suber, L *J. Chem. Soc., Dalton Trans.* **1993**, 2373.

M. MacKinetics cannot tolerate more than one kind of concentration unit (i.e., all concentrations must be in terms of molarity, pressure, or other appropriate units). Because a gas, H_2, is included in the kinetic model, the previously developed concept of a "hydrogen reservoir",[8,50] which converts the hydrogen pressure into a mathematically equivalent "molarity", needed to be employed. Put another way, the "hydrogen reservoir" is a way to treat pressures as if they were molar concentrations, but in a way that maintains the experimentally correct (known) amount of H_2 in solution for a given solvent and at a specified pressure. Using the "hydrogen reservoir" concept and using the conditions of the experiment shown in Figure 2 (except for the H_2 pressure, for which 40 psi was assumed) gives an $[H_2(\text{reservoir})]_i$ of 3.6 M (see page 144 of ref 50), and this is the initial value used for the concentration of $H_{2(gas)}$ in Scheme 2. The concentrations of all the other species is zero at $t = 0$.

The rate constants used for the kinetic model shown in Scheme 2 were chosen in the following way. (All the rate constants in Scheme 2 have time units of h and concentration units of M.) The values of k_f' and k_r' were made large in comparison to the other rate constants to avoid H_2 gas-to-solution "mass transfer" limitations[12] (our cyclohexene hydrogenation experiments are purposefully run under conditions that avoid mass transfer limitations[12]). The ratio of k_f' to k_r' was determined by the "hydrogen reservoir"[8,50] concept, which takes into account the known solubility of hydrogen in acetone.[51] The value of k_1' (in h^{-1}) was made small relative to k_2'[**A**] (also in h^{-1}) because autocatalytic surface growth is known to be faster than nucleation. The values of k_1' and k_2' were also adjusted to avoid a significant amount of $M(0)_{45}$ formation within the time required to hydrogenate all of the cyclohexene. (The formation of $M(0)_{45}$ is undesirable because it obscures the desired autocatalytic nature of the kinetic model; recall that the $M(0)_{45}$ species cannot grow any larger in this model, so autocatalytic surface growth can no longer take place for this species.) The values of k_1' and k_2' used in Scheme 2 lead to the formation of only a small amount of $M(0)_{45}$ near the end of the alkene hydrogenation (see Figure F of the Supporting Information). The value of k_{46}', the rate constant for the first alkene hydrogenation reaction, was made large relative to k_2' because alkene hydrogenation is being used as a fast reporter reaction for nanocluster growth. The values of $k_3'-k_{45}'$ and $k_{47}'-k_{90}'$ were determined relative to k_2' and k_{46}', respectively, as described in detail in the Supporting Information (i.e., by taking into account the changing fraction of surface atoms).

The alkene hydrogenation curves resulting from the numerical integration were curve-fit in exactly the same way as our experimental data (shown in Figure 2, for example). The curves were imported into Origin and only the first half of the alkene loss was used for the curve fit. Also, the reported values for $k_{2(\text{hydrogenation,corrected})}$ have been corrected for the stoichiometry factor and for the scaling factor (see the Supporting Information or our original treatment elsewhere[8]).

The Discovery of the Importance of Heterolytic Hydrogenation Activation—and the Need To Add Base To Initiate Nanocluster Formation—from Cationic Metals Such as Ru(II). The hydrogenation experiments with the precatalyst $[Bu_4N][Ru(1,5\text{-}COD)(CH_3CN)(P_3O_9)]$ were performed in the same manner as the hydrogenation experiments described above in the section labeled "Hydrogenations". In the drybox 5.4 (±0.1) mg of $[Bu_4N][Ru(1,5\text{-}COD)(CH_3CN)(P_3O_9)]$ was dissolved in 2.5 mL of 95% ethanol and 0.5 mL of cyclohexene, forming a clear, pale yellow solution. The $Bu_4N^+OH^-$ base was added at this point with a 50-μL syringe. For the experiment with 2.0 equiv of base, 15 μL of 1.0 M $Bu_4N^+OH^-$ was added. For the experiment with 1.0 equiv of base, 15 μL of 0.5 M $Bu_4N^+OH^-$ was added. Addition of base caused no noticeable change in the solution's appearance. The pale yellow solution was transferred into a new 22 × 175 mm Pyrex culture tube containing a $^5/_8 \times {}^5/_{16}$ in. stir bar. The culture tube was placed in a Fischer–Porter pressure bottle modified with Swagelock TFE-sealed Quick-Connects. The pressure bottle was then sealed, brought out of the drybox, placed in a 50 °C temperature controlled water bath, and connected to a H_2 line via the Quick-Connects. The pressure bottle was then purged 15 times (waiting 15 s between purges) with 40 psig H_2. Following the purges, the pressure bottle was pressurized to 40 ± 1 psig H_2. During the purging (and during the hydrogenation reaction) the reaction solution was vortex-stirred. Five minutes after, the beginning of the purges was designated $t = 0$, and at this time data collection was initiated using an Omega PX-621 pressure transducer interfaced to a PC.

During the hydrogenation experiment with $[Bu_4N][Ru(1,5\text{-}COD)(CH_3CN)(P_3O_9)]$ in the absence of base, the reaction solution remained clear and pale yellow. For the experiments with added base, the reaction solution became cloudy and brown and yielded an insoluble dark-colored precipitate. A TEM of the experiment with 2.0 equiv of base showed the presence of micrometer-scale particles, presumably bulk metal (see Figure K of the Supporting Information).

Acknowledgment. The TEMs for this work were obtained with the expert assistance of Dr. Eric Schabtach at the University of Oregon's Microscopy Center. Dr. Nicola E. Brasch is acknowledged for her advice concerning commercial nonlinear least-squares curve-fitting software. We also wish to thank Professor Steven H. Strauss at Colorado State University for allowing us to use his high-vacuum line for the H_2 uptake experiments. Financial support was provided by the Department of Energy, Chemical Sciences Division, Office of Basic Energy, Grant DOE FG06-089ER13998.

Supporting Information Available: Text describing a key control experiment demonstrating that the more direct monitoring of Ir(0) nanocluster formation by the GLC-determined evolution of cyclooctane gives identical rate constants, k_1 and k_2, within experimental error. Text describing the data analysis for cyclohexene hydrogenation experiments and how the changing fraction of nanocluster surface atoms is handled (i.e., the "scaling factor"). Figure A showing a detailed schematic of the high-vacuum gas-uptake apparatus used to measure H_2 uptake from the reduction of **A** in the absence of substrate. Figure B showing a histogram of nanocluster sizes when isolated after 50 min under H_2 and after 20 h under H_2. Figure C showing the hydrogen uptake curve for the "standard conditions" cyclohexene hydrogenation experiment where a TEM sample was removed after 30 min. Figure D showing the curve fit generated in Origin to a "mock" data set. Text describing, in the kinetic modeling, the "Treatment of the Changing Fraction of Surface Atoms by the Relative Values of $k_2'-k_{90}'$" plus the actual program used for the kinetic modeling experiment in MacKinetics. Figure E showing the results of the kinetic modeling program if a "critical nucleus" size of $M(0)_{13}$ is used. Figure F showing the concentration vs time curves for several $M(0)_x$ species in the kinetic modeling experiment. Figures G, H, and I showing GLC and ^{1}H NMR confirmation that the acetone solvent is hydrogenated by the Ir(0) nanoclusters to form 2-propanol. Text showing a mathematical treatment of the solvent vapor pressure correction. Figure J showing the sigmoidal hydrogen uptake curve for the hydrogenation of benzene with $TBA_5Na_3(COD)Rh{\cdot}P_2W_{15}Nb_3O_{62}$ as the precatalyst. Figure K showing a TEM of the reaction solution following a cyclohexene hydrogenation with the precatalyst $[Bu_4N][Ru(COD)(CH_3CN)(P_3O_9)]$ in the presence of 2 equiv of TBA^+OH^- (PDF). This material is available free of charge via the Internet at http://pubs.acs.org.

CM0006852

(50) Lyon, D. K. Ph.D. Dissertation, University of Oregon, 1990; see pp 142–145.

(51) The solubility data for H_2 in acetone is from *The Matheson Unabridged Gas Book*; *Hydrogen*; Matheson: East Rutherford, NJ, 1974.